Speeding up rendering of hybrid surface and volume models

Ferré, M. and Puig, A. and Tost, D.

Research Report LSI-03-53-R

Departament de Llenguatges i Sistemes Informàtics

UNIVERSITAT POLITÈCNICA DE CATALUNYA

Speeding up rendering of hybrid surface and volume models

Maria Ferré
URV Computer Science and Math. Dept.

Anna Puig Dani Tost
CREB Center of Biomedical Engineering Research, ETSEIB, UPC

Abstract

Hybrid rendering of volume and polygonal model is an interesting feature of visualization systems, since it helps users to better understand the relationships between internal structures of the volume and fitted surfaces as well as external surfaces. Most of the existing bibliography focuses at the problem of correctly integrating in depth both types of information. The rendering method proposed in this paper is built on these previous results. It is aimed at solving a different problem: how to efficiently access to selected information of a hybrid model. We propose to construct a decision tree (the Rendering Decision Tree), which together with an auxiliary run-length representation of the model avoids visiting unselected surfaces and internal regions during a traversal of the model.

Keywords Volume Rendering, Hybrid Rendering, Decision Tree, Run-length encoding.

1 INTRODUCTION

There are two main approaches of the visualization of voxel models: rendering the volume as a whole and rendering isosurfaces. The former approach is achieved by Direct Volume Rendering (DVR), which computes the contribution of all the voxels to the image. Indirect Volume Rendering (IVR) can perform the latter approach. Isosurfaces are first extracted from the volume data with the popular Marching Cubes algorithm [LC87], or by contouring and slicing [MSS92]. Then, they are rendered with the standard hardware-assisted polygon- rendering pipeline. Alternatively, Direct Volume Rendering (DVR) [Lev90] can also render surfaces, by computing the contribution to the image of the volume cells that contain the isosurfaces, and applying a surface shading without need of intermediate representations. The major advantage of IVR to visualize surfaces is that, once the polygonal model is extracted, its rendering is generally faster than DVR, even if its number of faces is large. In addition, any level of zoom can be applied during IVR rendering, whereas the lack of an actual polygonal model in DVR reduces its suitability when the surface is very near the observer. However, DVR does not require any preprocessing step and, thus, it provides more flexibility to visualize different isosurfaces.

Combining the two approaches, i.e. mixing surface and volume rendering is an interesting feature of volume visualization. It conveys more information than only surfaces but in a neater way than volume only. Therefore, it provides a better perception of the relationships between the different regions of the data. Mixing surfaces and volumes can also be used to show the interaction of external synthetic surfaces with a volume, as for example CAD models of a scalpel, bone prosthesis or a radiation beam with MR data or CT data.

DVR provides a natural way to mix surface and volume rendering by applying different shading models to the cells depending on if they belong to the boundary of a feature or to its interior. In this paper, we call *hybrid shading* this rendering modality. Moreover, hybrid shading can be extended to external surfaces by voxelizing them in a pre-process [Kau87]. A similar approach has been used for realistic rendering of complex scenes with a huge number of faces and repetitive patterns such as forests, in which trees and leaves can be represented with geometrical models if they are near or as a voxelization storing BRDF's if they are

far [Nom95] [Ney98]. However, this type of rendering requires a low ratio image pixel per voxel, because it does not have a polygonal model of the surfaces.

An alternative to the voxelization is to keep separate representations of the volume and the surfaces (fitted as well as external) or a hybrid model representing both types of data, and to mix them during rendering. We will call *hybrid rendering* this approach to distinguish it from *hybrid shading*. Existing methods following this approach are based on ray casting [Lev90] [Fru91] [MK92] [SK94], Z-Buffer and Back-to-Front traversal [GMO89] [KYC90] [Eck99] [TPN93] and 3D texture-mapping [KK99] [BN03]. They are reviewed in the next section.

Most of the existing hybrid rendering methods focus mainly at solving the problem of correctly depth sorting the volume samples and the polygons. They assume that all the volume and the surfaces must be rendered and thus, they essentially visit all the data. This is inefficient when not all the volume and not all the surfaces must be rendered, which is often the case in the exploration of a dataset. In fact, a desirable feature of hybrid rendering is the flexibility to render specific regions of the data, either their surface, their internal volume or both, while hiding others.

Trying to restrict the traversal of a volume data set to the relevant cells is a general problem in volume visualization. It has been addressed for the acceleration of isosurfacing (octrees [WG92], span space [LSJ96]) as well as for speeding up volume rendering (kd-trees [SF90], octrees [WG94], run-length encoding [LL94]). However, as mentioned above, this problem has been little addressed in hybrid rendering [Lev90].

This paper addresses the problem of the fast exploration of hybrid models. Our primary goal is provide means of performing efficiently various visualizations of the models, changing the selection of the features to be rendered. We assume that the original model has been classified. Therefore, our method is not suitable for a first exploration of a dataset, but rather to efficiently manipulate it once its internal structure is known. The main application of our method is teaching by rendering atlas or case study models. It is suitable for *hybrid shading* with low ratio pixel/voxel as well as for *hybrid rendering* when zooming on the surfaces is required.

In the next section, we review the previous work on hybrid rendering. Next, we describe the proposed model and the traversal algorithm associated to it. Finally, we show the results of the simulations and the conclusions.

2 PREVIOUS WORK

Ray casting can handle simultaneously different models by tracing the ray against each of them and merging their contribution along the ray. Based on this strategy, the hybrid ray tracer proposed by Levoy [Lev90] reduces the aliasing problems near the surfaces by performing an adaptive sampling of the volume. Miyazawa and Koyamada [MK92] improved the antialiasing by first classifying the surface inside the volume. For each voxel, they compute a list of intersecting polygons. Therefore, the voxels with a non-empty list of polygons can be over sampled when rays are cast. Fruhauf [Fru91] also proposes the use of ray casting for volume, combined with any rendering algorithm for the geometric primitives capable of outputting an image space sorted list of elements that can be merged along the rays. Sobierajski and Kaufman [SK94] designed a general ray tracer capable of handling various surfaces and volume models. They propose a classification of the intersection types that, together with the use of bounding boxes for the objects, avoid useless intersection tests and volume sampling of occluded regions.

Z-Buffer has also been extended to mixed surfaces [GMO89], [KYC90]: two independent Z-buffer processes are realized and then, the image buffers are combined according to their associated depths. A similar idea is used in *Volumizer* [Eck99]. The disadvantage of these approaches is that they cannot handle correctly semi-transparent volumes and transparent surfaces simultaneously. In a different approach [TPN93], the synthetic surface is converted into a face-octree representation according to the orientation and resolution of the voxel model. The face-octree is traversed back-to-front simultaneously with the voxel model preserving the correct depth order and thus allowing transparency of both the volume and the surface.

More recently, a 3D texture-map-based volume rendering approach has been proposed, able to render

opaque and translucent polygons together with semi-transparent volume at interactive rates [KK99]. The volume is processed in a slice-by-slice basis. The volume slices and the translucent polygons clipped at the boundary of the slabs defined by two consecutive slices are rendered alternatively, preserving a correct depth composition. In order to avoid costly clipping operations of the polygons against the slices, the authors propose to use a bucket sort of the translucent polygons according to the slabs that they traverse. This strategy has also been used [BN03] in order to render a hybrid octree which encodes the volume as well as the surface. The major advantage of the hybrid octree is that the texture associated to the volume can be generated at different levels of resolution depending on the variation of the scalar field in the node or its relative importance to the visualization. This characteristic simplifies the sorting of the surface polygons between slices, and it can be used to obtain multiresolution hybrid visualizations.

Levoy addresses the problem of avoiding irrelevant data during hybrid rendering in the paper mentioned above [Lev90]. Levoy proposes to use an octree representation of the volume to efficiently skip over empty regions. However, as the surface model is kept separately from the volume, this method does not provide a fast way of accessing directly to voxels traversed by an external surface or containing a given isosurface. The face octree proposed in [TPN93] grants a fast access to the codified surface voxels but it is restricted to the codification of only one external surface and it does not classify the volume into regions. The hybrid octree described by Boada at al. [BN03] provides also a fast access to surface nodes. In addition, similarly to the BON structure [WG92], it stores the maximum and minimum values of each node and thus, it provides means of skipping over non-relevant nodes of the volume. However, it is restricted to one fitted surface. Finally, sorting intersection elements as proposed by Sobierajski at al. [SK94] can avoid traversing occluded voxels or computing unnecessary intersections ray surfaces but it does not eliminate unwanted traversals.

3 THE PROPOSED METHOD

3.1 The Rendering Decision Tree (RDT)

Our work is inspired on the *Decision Trees*, well known in the Information Theory field [GS88]. When rendering a scene, in general as well in volume and hybrid rendering, users must select and specify properties of the objects (or voxels) that should actually be visualized. This selection can be viewed as *feature vector* of a multidimensional feature space, in which the objects of a scene (voxels in a volume model) can be classified into semantic regions. Rendering queries are hardly arbitrary but rather follow the semantic structure of the scene. If this structure is known, it can be used to construct a decision tree, the *Rendering Decision Tree(RDT)* that will allow us to quickly determine the set of selected objects or voxels.

In the initial exploration of a voxel model, users select relevant ranges of values by conveniently specifying transfer functions [KKH01] that set to zero the opacity of the other value ranges. Thus, in the rendering, although all the volume is traversed, non-relevant regions are hidden. Let n be the number of voxels of a volume model. In order to render the model, only a subset of k voxels actually contribute to the image: those that fulfill the rendering specifications, i.e. those that belong to the selected class. Once the model has been classified, successive visualizations will drive to the selection of subsets within this classification. Traversing all the volume when these classes have already been characterized results in unnecessary visits to $n-k$ remaining voxels. The aim of the RDT is provide a direct access to the selected subsets corresponding to the different classes.

Figure 1 shows an example of a RDT for a model of the brain. It classifies the brain into three regions: the right and left hemispheres cortex and the cerebellum. Each of these regions is subdivided into two categories: boundary and interior. The internal regions of the hemispheres are in turn classified into other structures, which again separate the boundary from the interior. If, as an example, the user wants to render the surface of the cerebellum of the right hemisphere together with the volume of the left hemisphere, the tree is traversed and voxels that belong to these classes are selected for rendering. In the next section we discuss how to associate to each node of such a tree the corresponding information of the model.

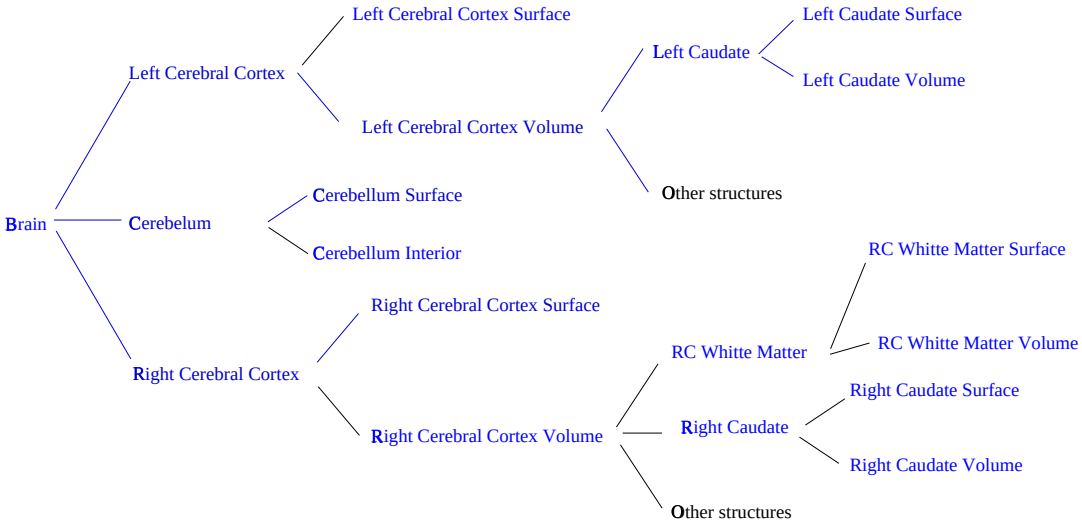

Figure 1: RDT Example for a model of the brain. Selected areas to be rendered are colored in blue.

3.2 The run-length encoding

Our method is suitable for hybrid shading as well as hybrid rendering. In both cases, we take as input the original voxel model. We use the classification step to construct an RDT that classifies the voxels into regions and into internal and boundary voxels. For hybrid shading, we first extract the relevant isosurfaces from the voxel model by applying a Marching Cubes algorithm. Each boundary voxel points to as many lists of polygons as extracted isosurfaces cross it. Furthermore, if a synthetic surface must be mixed with the volume, we classify and clip it with the volume cells as if it is a fitted surface.

A naive approach in order to associate to the RDT nodes the set of corresponding voxels is to keep a simple list of voxels per node. This approach presents serious drawbacks. First, being each list independent from the order, this model would not preserve the spatial ordering inherent to the voxel model between the different classes. Moreover, this structure would have huge memory occupancy, as it would require for each non-empty voxel one pointer per region to which it belongs.

We propose to construct an auxiliary voxel model that labels each voxel according to the leave of the RDT to which it belongs. We use a Run-Length (RL) codification of this model. Each leave of the RDT stores the label of its associated class in the RL model. Therefore, when a rendering selection is done, the RDT is traversed in order to compute the labels of the selected classes. If a terminal node matches the rendering criterion, its associated class is selected for rendering. If it is a non-terminal node that matches the rendering criterion, all its descendent classes are selected. The RL model is then traversed skipping over non-selected classes and accessing to the actual scalar or surface values of the voxels belonging to the selected classes only.

Figure 2 illustrates this process with a color codification. The voxel model has been classified according to the RDT tree shown at the right of the figure. The RL is depicted together with the classified voxel model. It should be observed that, for clarity, the voxel model depicted is the classified one, although in the voxel array, we actually keep the original gray values of the data. The traversal of the RDT selects the blue and red voxels. The run-length traversal skips over the other colors, and accesses to the actual scalar and surface values of only the blue and red voxels.

The traversal of the RL preserves the order of the voxel model, so it can be used for BTF and FTB traversals of the model, for splatting, shear-warp, or in order to compute 3D-texture maps of the model. However, it is not convenient for ray casting, as it does not provide a direct access to the voxels individually. As its primary goal is to speed up rendering, and being ray casting a slow method, this is not a major drawback. It should be observed that, if the camera rotates around the model, three run-length codifications must be

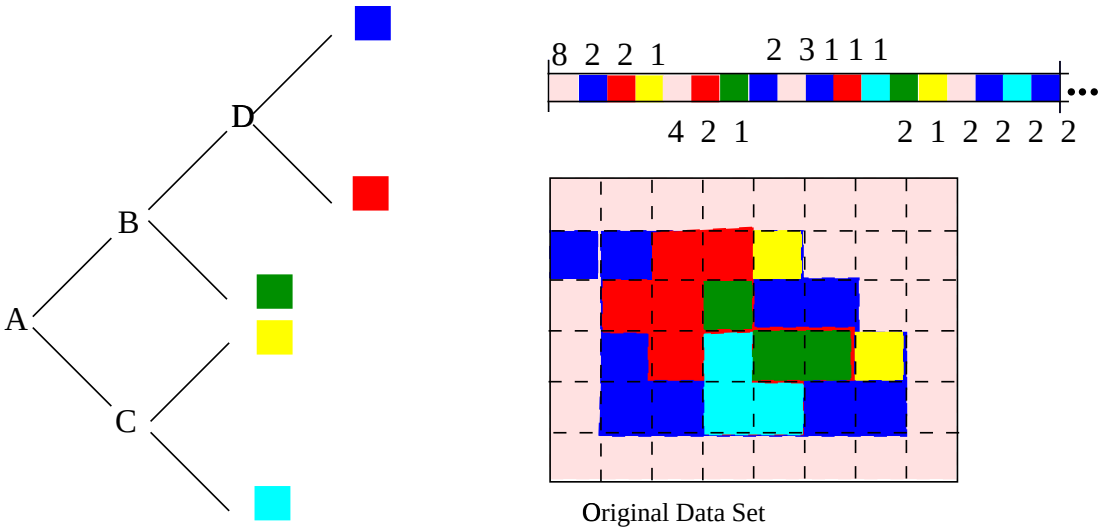

Figure 2: RL model based on the RDT labeling. At right, the RDT is depicted labeling the internal nodes with a letter and the leaves with a color. At bottom left, the classified voxel model is shown, and at top left top, its RL codification.

computed corresponding to the three axes order permutations.

It should be observed that, if a unique run-length model is constructed, each voxel must belong to only one leave of the RDT. This means that the classification process must partition the data into disjoint regions or into regions enclosed one into each other following the hierarchy of the RDT. This cannot be guaranteed if the classification criterion separates the boundary voxels of each surface into different classes, since boundary voxels may be crossed by more than one isosurface. However, this problem can be avoided if the RDT classifies voxels into different groups according to the combination of surfaces that cross them. As a consequence, nodes of a tree can share descendents. Specifically, nodes representing adjacent semantic regions can share a descendent node representing the voxels crossed by the boundaries of these regions. Figure 3 illustrates such a structure. The RDT classifies the voxels into 9 regions: interior voxels (I1, I2, I3), voxels crossed by only one surface (B1, B2, B3) and voxels crossed by more than one surface (B1/B2, B1/B2/B3). The drawback of this solution is that it increases the number of classes and, therefore it may result in a higher fragmentation of the RL and thus, higher memory requirements. In order to solve this problem, instead of one RL model, several RL could be created, associated to the intermediate nodes of the RDT and traversed simultaneously. We are currently working on these types of structure, but the results shown in the next section correspond only to the former one.

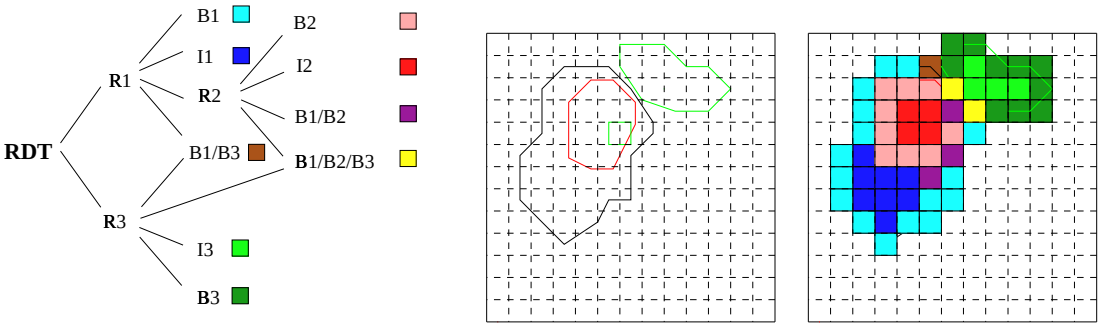

Figure 3: Example of an RDT labeling with multiple surfaces crossing voxels. The RDT tree is depicted at the left; the regions in the voxel model at the middle and the labeling of the voxels in the RL at the right.

3.3 Rendering

As mentioned above, our model is suitable for sorted traversals of the data. In our simulations, we have used it to render the model using the splatting strategy. The traversal of the run-length models accesses to the selected voxels, which can fall into three categories, depending on the visualization query: interior voxels, surface voxels and hybrid voxels. The former ones are purely volumetric. They are splatted according to their emission and absorption. When a surface voxel is reached, the polygons inside it are projected. It should be noted that if more than one surface crosses the voxel and the surfaces are translucide, the order of the projection of the polygons is relevant. We use the approach proposed by Kreeger and Kaufman [KK99] to solve this problem, using the GL z-tests. Finally, for the third type of voxels, we first project the surface and next splatt the interior. As in other previous approaches, this actually composes erroneously the surface and the volume. Removing this error would require knowledge of the decomposition of the voxel into subvolumes according to the surfaces that cross it. We do not address this problem in this paper.

4 RESULTS

All the simulations have been carried out on a Sun Ultra 60 360MHz using our multimodal rendering software platform Hipo [PTF02]. For all the simulations, we have first executed a non-optimized version of the traversal algorithm using the original voxel model without RDT and RL. This rendering serves us as the unit of CPU cost. All the CPU costs shown in the tables are relative to this unit cost in order to effectively measure the improvements provided by the proposed method.

Two datasets have been used: a 32x32x32, one byte intensity phantom model and a real dataset composed of 190x220x178 MR (Magnetic Resonance) data of the brain. The phantom model is composed of two disjoint voxelized spheres. The surfaces of these spheres have been extracted using a Marching Cubes algorithm. The RDT subdivides the volume into these two regions at the first level of the tree, and into interior and boundary regions at the second level. Figure 4 shows several rendered images of this model, selecting either the two surfaces, the two internal regions or mixing surfaces and volume. Table 1 gives information on the size of the model, its internal regions and the number of triangles of the surfaces.

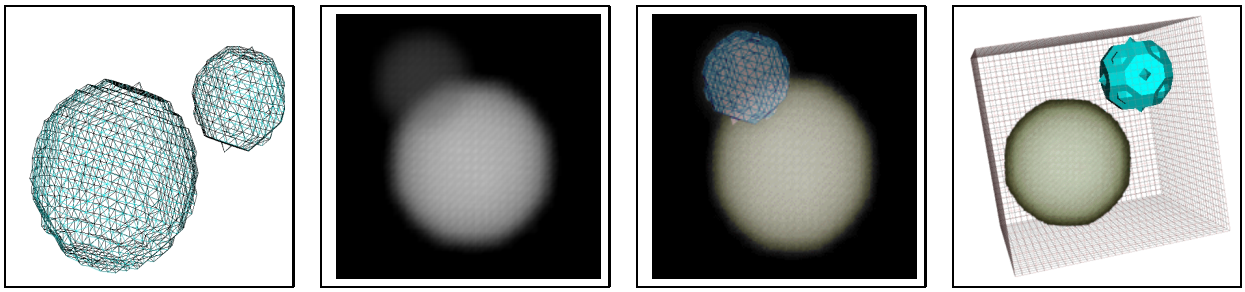

(a) (b) (c) (d)

Figure 4: Different images of the phantom model: (a) Triangle meshes of the extracted fitted surfaces, (b) Volume rendering, (c) Hybrid rendering of the volume of two regions and the wireframe surface of one region, (d) Hybrid rendering of one region of the volume and the shaded surface of the other region framed into the voxel model.

	Subtree Sphere 1	Subtree Sphere 2	Global model
Interior voxels	2.705	437	3.142
Boundary voxels	1.440	464	1.904
Empty voxels			27.722
Surface triangles	3.704	1.352	5.056

Table 1: Description of the Phantom hybrid model.

Table 2 shows the cost of different traversals of the proposed model in comparison to full traversals of the structure. The simulations correspond to the images shown in Figure 4.

Subtree 1	Subtree 2	kvol	ksur	khyb	occupancy ratio	rendering ratio
Surface	Surface	0	1904	0	0.0581	0.2831
Volume	Volume	5046	0	0	0.0958	0.3595
Volume	Both	437	1440	464	0.0714	0.3253
Surface	Volume	4145	464	0	0.1406	0.3629

Table 2: Simulation results on the Phantom model. The first two columns indicate the branch of each subtree that has been visualized (volume, surface or both). The next three columns indicate the number of selected voxels for each category: volume voxels (kvol), surface voxels (ksur) and hybrid voxels (khyb). Column 6 indicates the relative occupancy of the selected features, i.e. kvol+ksur+khyb divided by the total occupancy of the model 32768. Column 7 shows the relative cost of the rendering in relation to the cost of the same rendering without using the proposed structure.

Similar simulations have been performed on the MR model of a human head as shown in 5 and 6. In some figures, we have rendered the regions with a constant color, and in some others we have used the gray value of the model. In the former case, it is only necessary to traverse the RL model, since it is not required to access to the actual voxel array. However, in order to have comparable results in the simulations, we have performed this access for all selected voxels. The RDT is composed of two main branches: the brain, which is subdivided into regions as depicted in the RDT of Figure 1 and the rest of the head. The fitted surfaces correspond to the regions labeled as: right cerebral cortex, right cerebral white matter, left and right caudate, left cerebral cortex and left and right cerebellum cortex. Table 3 shows the occupancy of these regions in terms of number of voxels and surface triangles. The simulation results are listed in Table 4.

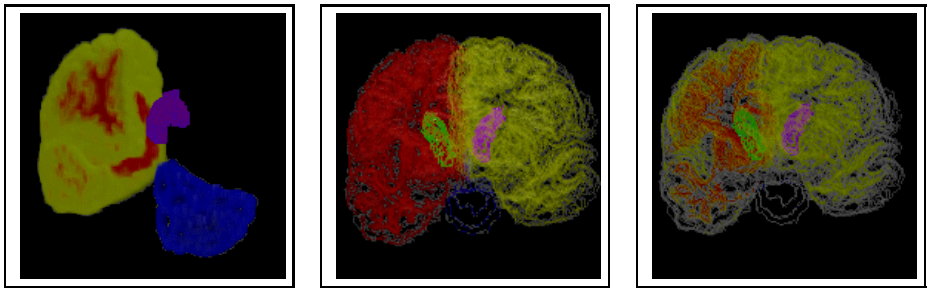

(a) (b) (c)

Figure 5: Rendered images of the brain model. (a) volume of the left caudate, volume of the right cerebral cortex and the right cerebral white matter and surface of the left cerebellum cortex, (b) surfaces of the left and right cerebral cortex and of the left and right caudate, (c) same surfaces as (b) plus surface and volume of the right cerebral white matter.

Region	Interior voxels	Boundary voxels	Surface triangles
Right cerebral cortex	511036	77792	382609
Right cerebral white matter	165956	103513	256691
Right caudate	1462	2693	7056
Right cerebellum cortex	60600	16410	52430
Left cerebral cortex	509588	83890	388824
Left caudate	1588	2576	6609
Left cerebellum cortex	60484	16664	53871
Non-brain head region	4423855	464540	958439

Table 3: Description of the MR labeled model of the brain.

The relative cost of our method, in comparison to full traversal, ranges between 20% and 30% for the phantom model and 20% and 70% for the head model. This is an important speedup of the rendering. Taking

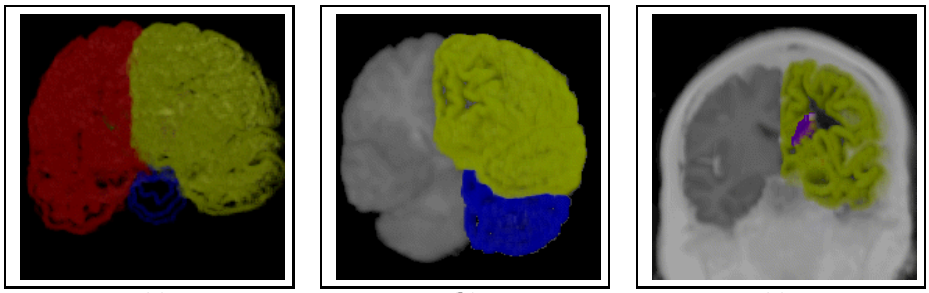

(a) (b) (c)

Figure 6: Rendered images of the brain model. (a) surface and volume of the right and the left cerebral cortex and surfaces of the right and the left cerebellum cortex, (b) volume of the right cerebral cortex and the right cerebellum cortex and surface and volume of the left cerebral cortex and the left cerebellum cortex, (c) volume of the non-brain voxels of the head and of the right cerebral cortex, volume of the left caudate and surface of the left cerebral cortex.

Figure	kvol	ksur	khyb	Occupancy ratio	Rendering cost ratio
5.a	879125	0	0	0.118	0.294
5.b	0	166951	0	0.224	0.194
5.c	332907	0	103513	0.058	0.291
6.a	1020624	106301	161682	0.172	0.469
6.b	1235910	0	100554	0.179	0.447
6.c	4936479	83890	0	0.674	0.867

Table 4: Simulation results for the MR head dataset. The first column indicates the corresponding figure; the three next columns show the number of volume voxels (kvol), surface voxels (ksur) and hybrid voxels (khyb); Column 5 shows the ratio of occupancy of the selected features in terms of number of selected voxels divided by the size of the model 190x220x178; Column 6 shows the ratio of cost of our implementation in relation to full traversal of the model for the same selection.

into account that the cost of creation of the structure in relation to the basic rendering cost is 0.49, the proposed method speeds up the rendering, even for only one traversal. It should be noted that this reduction in the cost is attributable to the efficiency of the proposed traversal, since the rendering cost itself (shading, projecting and compositing in the selected voxels) is the same in our method as a in full traversal. However, the rendering cost influences the overall improvement of the method, as it is part of the total cost. This explains the variation of the cost ratio, depending on the number, type of selected voxels and number of triangles per voxels. The efficiency of our method is due to the fact that the occupancy ratios are low, at most 30% in the five first simulations on the head model, which is not a biased data, since the simulations correspond to real physician's queries. The worst efficiency is obtained in the last simulation in which almost 70% of the voxels are selected. We expect the occupancy of relevant features to be low in other applications. This observation was the primary motivation of our work.

5 CONCLUSIONS

The method proposed in this paper is aimed at speeding the traversal of hybrid classified models. The Rendering Decision Tree (RDT) together with the auxiliary Run-Length encoding (RL) of the model provides means of accessing directly to the regions and the surfaces selected for rendering avoiding unnecessary traversals of the entire model. The simulations performed show that the method can improve the efficiency of the traversal in 60 to 70 % percent. Several development stem from this work. First, we would like perform more measurements of the relative efficiency of our structure in comparison to substituting the auxiliary RL model by multiple overlapping less fragmented RL at different levels of the tree. Comparison of its efficiency with octree structures are also desirable. In addition, more work should be done to enhance the depth composition

for zooming on boundary voxels crossed by one or more surfaces. Finally, we are currently investigating means of reducing the IO operations for successive rendering with a similar rendering selection.

Acknowledgments: This work has been funded by the project MAT2002-04297-C03-02 from the Ministerio de Educación y Ciencia.

References

[BN03] I. Boada and I. Navazo. 3D texture-based hybrid visualizations. *Computers and Graphics*, (27):41–49, 2003.

[Eck99] G. Eckel. OpenGL volumizer programmer's guide. *Document n. 0073720001*, 1999.

[Fru91] M. Fruhauf. Combining volumen rendering with line and surface rendering. In *Proceedings of Eurographics'91*, pages 21–32. Elvesier Science Publisher (North Holland), 1991.

[GMO89] D.S. Goadsell, S. Mian, and A.J. Olson. Rendering volumetric data in molecular systems. *Journal of Molecular Graphics*, 7, March 1989.

[GS88] R.M. Goodman and P. Smyth. Decision tree design from a communication theory standpoint. *IEEE Transactions on Information Theory*, 34(5):979–994, 1988.

[Kau87] A. Kaufman. Efficient algorithms for 3D scan-conversion algorithms of parametric curves, surface and volumes. *ACM Computer Graphics*, 21:171–179, July 1987.

[KK99] K. Kreeger and A. Kaufman. Mixing translucent polygons with volumes. *Proc. IEEE Visualization*, pages 191–198, 1999.

[KKH01] J. Kniss, G. Kindlmann, and C. Hansen. Interactive volume rendering using multi-dimensional transfer functions and direct manipulation widgets. In *Proceedings of the conference on Visualization 2001*, pages 255–262. IEEE Press., 2001.

[KYC90] A. Kaufman, R. Yagel, and D. Cohen. Intermixing surface and volume rendering. *3D Imaging in Medicine: Algorithms, Systems and Applications*, pages 217–228, 1990.

[LC87] W.E. Lorensen and H.E. Cline. Marching cubes: A high resolution 3D surface construction algorithm. *ACM Computer Graphics*, 21(4):163–169, July 1987.

[Lev90] M. Levoy. A hybrid ray tracer for rendering polygon and volume data. *IEEE Computer Graphics & Applications*, 10(8):33–40, March 1990.

[LL94] P. Lacroute and M. Levoy. Fast volume rendering using a Shear-Warp factorization of the viewing transformation. *ACM Computer Graphics*, 28(4):451–458, July 1994.

[LSJ96] Y. Livnat, H.W. Shen, and C.R. Johnson. A near optimal isosurface extraction algorithm using the span space. *IEEE Transactions on Visualization and Computer Graphics*, 2(1), March 1996.

[MK92] T. Miyazawa and K. Koyamada. A high-speed integrated renderer for interpreting multiple 3D volume data. *The Journal of Visualization and Computer Animation*, 3:65–83, 1992.

[MSS92] D. Meyers, S. Skinner, and K. Sloan. Surfaces from contours. *ACM Transactions on Graphics*, 11(3):228–258, 1992.

[Ney98] F. Neyret. Modeling, animating and renedering complex scenes using volumetric textures. *IEEE Transcations on Visualization and Computer Graphics*, 4(1):55–70, 1998.

[Nom95] T. Noma. Bridging between surface rendring and volume rendering for multiresolution display. In *Proceedings of the 6th Eurographics Workshop on Rendering*, pages 57–67. Eurographics, 1995.

[PTF02] A. Puig, D. Tost, and M. Ferré. Design of a multimodal rendering system. *Proc. 7th International Fall Workshop Vision, Modeling and Visualization 2002, Greiner G,. Niemann, H., Ertl, T., Girod, B. and Seidel, HP. Editors*, pages 488–496, 2002.

[SF90] K.R. Subramanian and D.F. Fussell. Applying space subdivision techniques to volume rendering. *Proc. Visualization'90*, pages 150–159, 1990.

[SK94] L.M. Sobierajski and A. Kaufman. Volumetric ray tracing. *Proc. 1994 Symposium on Volume Visualization*, october 1994.

[TPN93] D. Tost, A. Puig, and I. Navazo. Visualization of mixed scenes based on volume and surface. *Proc. European Workshop on Rendering*, pages 281–294, 1993.

[WG92] J. Wilhems and A. Van Gelder. Octrees for faster isosurface generation. *ACM Transactions on Graphics*, 11(3):201–227, July 1992.

[WG94] J. Wilhems and A. Van Gelder. Multidimensional trees for controlled volume rendering and compression. *Proc ACM Symposium on Volume Visualization*, 11:27–34, October 1994.

Departament de Llenguatges i Sistemes Informàtics
Universitat Politècnica de Catalunya

Research Reports - 2003

- LSI-03-1-R : *Metaheuristics for the Edge-Weighted $-Cardinality Tree Problem* , Blesa, M.J. and Blum, C.
- LSI-03-2-R : *Organizational and National Issues of an ERP Implementation in a Portuguese Company* , Alvaro, J. and Esteves, J. and Pastor, J.A.
- LSI-03-3-R : *A Complete Solid Model for Surface Rendering* , Aguilera, A. and Ayala, D. and Rodríguez, J.
- LSI-03-4-R : *Fast Neighborhood Operations for Images and Volume Datasets* , Ayala, D. and Rodríguez, J.
- LSI-03-5-R : *A Review of Integrity Constraint Maintenance and View Updating Techniques* , Mayol, E. and Teniente, E.
- LSI-03-6-R : *Porqpine: A Peer-to-Peer Search Engine* , Bermúdez, J. and Pujol, J.M. and Sangüesa, R.
- LSI-03-7-R : *KDSM Methodology for knowledge discovery from a domain where repeated very short serial measures with a blocking factor are present* , Alvarado, G. and Cortés, U. and Gibert, K. and Rodas, J. and Rojo, J.E.
- LSI-03-8-R : *On the Maximum Common Embedded Subtree Problem for Ordered Trees* , Valiente, G.
- LSI-03-9-R : *Searching by approximate personal-name matching* , Camps, R. and Daudè, J.
- LSI-03-10-R : *Two triangulations methods based on edge refinement* , Ayala, D. and Pla, N. and Vigo, M.
- LSI-03-11-R : *Constrained Tree Inclusion* , Valiente, G.
- LSI-03-12-R : *Geometry of language and linguistic circuitry* , Morrill, G.
- LSI-03-13-R : *A simple yet useful approach to implementing UML Profiles in CASE tools* $ExtendedVersio$, Cabot, J. and Gómez, C.
- LSI-03-14-R : *Solving 'Still life' with Soft Constraints and Bucket Elimination* , Larrosa, J. and Morancho, E.
- LSI-03-15-R : *A fast hierarchical traversal strategy for multimodal visualization*, Puig, A. and Tost, D.
- LSI-03-16-R : *The complexity of deciding stability under FFS in the adversarial model* , Àlvarez, C. and Blesa, M.J. and Díaz, J. and Fernández, A. and Serna, M.
- LSI-03-17-R : *A Case Study on Building Conceptual Schemas by Refining General Ontologies* , Conesa, J. and de Palol, X.
- LSI-03-18-R : *Analysing similarity assessment in feature-vector case representations* , Comas, J. and Cortés, U. and Núñez, H. and Poch, M. and Rodríguez-Roda, I. and Sànchez-Marrè, M.
- LSI-03-19-R : *Análisis de medidas repetidas mediante el uso de la curva media como síntesis* ,

Cortés, U. and Gibert, K. and Rodas, J. and Rojo, J.E.

- LSI-03-20-R : *Statistical Strategies for Pruning All the Uninteresting Association Rules* , Casas, G.
- LSI-03-21-R : *Discovering Unbounded Episodes in Sequential Data* , Casas, G.
- LSI-03-22-R : *Query Containment with Negated IDB Predicates ExtendedVersion* , Farré, C. and Teniente, E. and Urpí, T.
- LSI-03-24-R : *Using concept lattices to mine functional dependencies* , Baixeries, J.
- LSI-03-25-R : *Adversarial models for prority-based networks* , Àlvarez, C. and Blesa, M.J. and Fernández, A. and Serna, M.
- LSI-03-26-R : *Characterization of Concept Lattices for Ordered Contexts* , Casas, G.
- LSI-03-27-R : *Computation of bisection width for random d-regular graphs* , Serna, M. and Serras, J. and Wormald, N.C.
- LSI-03-28-R : *Building and Using Quality Models for Complex Software Domains* , Carvallo, J.P. and Franch, X. and Quer, C.
- LSI-03-29-R : *Kernel Arquitecture for CAD/CAM in Shipbuilding Enviroments* , González, J. and Gurrea, I. and Rodríguez, A. and Solano, Ll.
- LSI-03-30-R : *Margin Maximization with Feed-forward Neural Networks: A Comparative Study with Support Vector Machines and AdaBoost* , Carreras, X. and Màrquez, Ll. and Romero, E.
- LSI-03-31-R : *Una notación algorítmica con genericidad y herencia junto con su relación con C++ y Java* , Mylonakis, N.
- LSI-03-32-R : *Study on k-Shortest Paths with Behavioral Impedance Domain from the Intermodal Public Transportation System Perspective* , Madriz-Lozada, E. and Pereira, H. and Perez, Ll.
- LSI-03-33-R : *On the Complexity of Resolution with bounded Conjunctions* , Borralleras, C. and Esteban , J.L. and Mossner, J.
- LSI-03-34-R : *Generic Algorithms for the Generation of Combinatorial Objects* , Martínez, C. and Molinero, X.
- LSI-03-35-R : *An Efficient Generic Algorithm for the Generation of Unlabelled Cycles* , Martínez, C. and Molinero, X.
- LSI-03-36-R : *CBR and MBR techniques: review for an application in the emergencies domain* , Mérida-Campos, C. and Rollón, E.
- LSI-03-37-R : *Using NLP tools in the Specification Phase* , Castell, N. and Hernández, A.
- LSI-03-38-R : *Classificació automàtica amb KLASS de les dades de procés d'una EDAR*, Flores, X. and Gibert, K. and Rodríguez-Roda, I.
- LSI-03-39-R : *VolumeEVM: A new surface/volume integrated model* , Ayala, D. and Rodríguez, J.
- LSI-03-40-R : *MKtrees: Construction and Applications* , Brunet, P. and Franquesa, M.
- LSI-03-41-R : *From Supply Chains to Demand NetworksȦgents in Retailing: The Electrical Bazaar* , Almirall, E. and Brito, I. and Cortés, U. and Silisque, A.

- LSI-03-42-R : *Fixed-Parameter Algorithms for the k, r-Center in Planar Graphs and Map Graphs* , Demaine, E.D. and Fomin, F.V. and Hajiaghayi, M. and Thilikos, D.M.
- LSI-03-43-R : *Dominating sets and local treewidth* , Fomin, F.V. and Thilikos, D.M.
- LSI-03-44-R : *Res2 Lower Bounds for Tseitin Formulas* , Bonet, M. and Esteban , J.L.
- LSI-03-45-R : *Collision Queries: Models and Algorithms* , Brunet, P. and Franquesa, M.
- LSI-03-46-R : *Collision Prediction Using MKtrees: Broad Phase and Refinement Levels of the Narrow Phase* , Brunet, P. and Franquesa, M.
- LSI-03-48-R : *Bidimensional Parameters and Local Treewidth* , Demaine, E.D. and Fomin, F.V. and Hajiaghayi, M. and Thilikos, D.M.
- LSI-03-50-R : *A distributed algorithm to find Hamiltonian cycles in Gnp random graphs* , Levy, J. and Louchard, G. and Petit, J.
- LSI-03-51-R : *A characterization of universal stability in the adversarial queuing model* , Àlvarez, C. and Blesa, M.J. and Serna, M.
- LSI-03-52-R : *Automatic Generation of Polynomial Loop Invariants for Imperative Programs*, Kapur, D. and Rodríguez, E.
- LSI-03-53-R : *Speeding up rendering of hybrid surface and volume models*, Ferré, M. and Puig, A. and Tost, D.

Hardcopies of reports can be ordered from:

Núria Sanchez
Departament de Llenguatges i Sistemes Informàtics
Universitat Politècnica de Catalunya
Campus Nord, Mòdul C6
Jordi Girona Salgado, 1-3
03034 Barcelona,Spain
nurias@lsi.upc.es

See also the Departament WWW pages, http://www.lsi.upc.es/